Quantum Science and Technology



**PAPER** • **OPEN ACCESS**

# Quantum lattice Boltzmann algorithm for heat transfer with phase change

To cite this article: Christopher L Jawetz *et al* 2026 *Quantum Sci. Technol.* **11** 035032



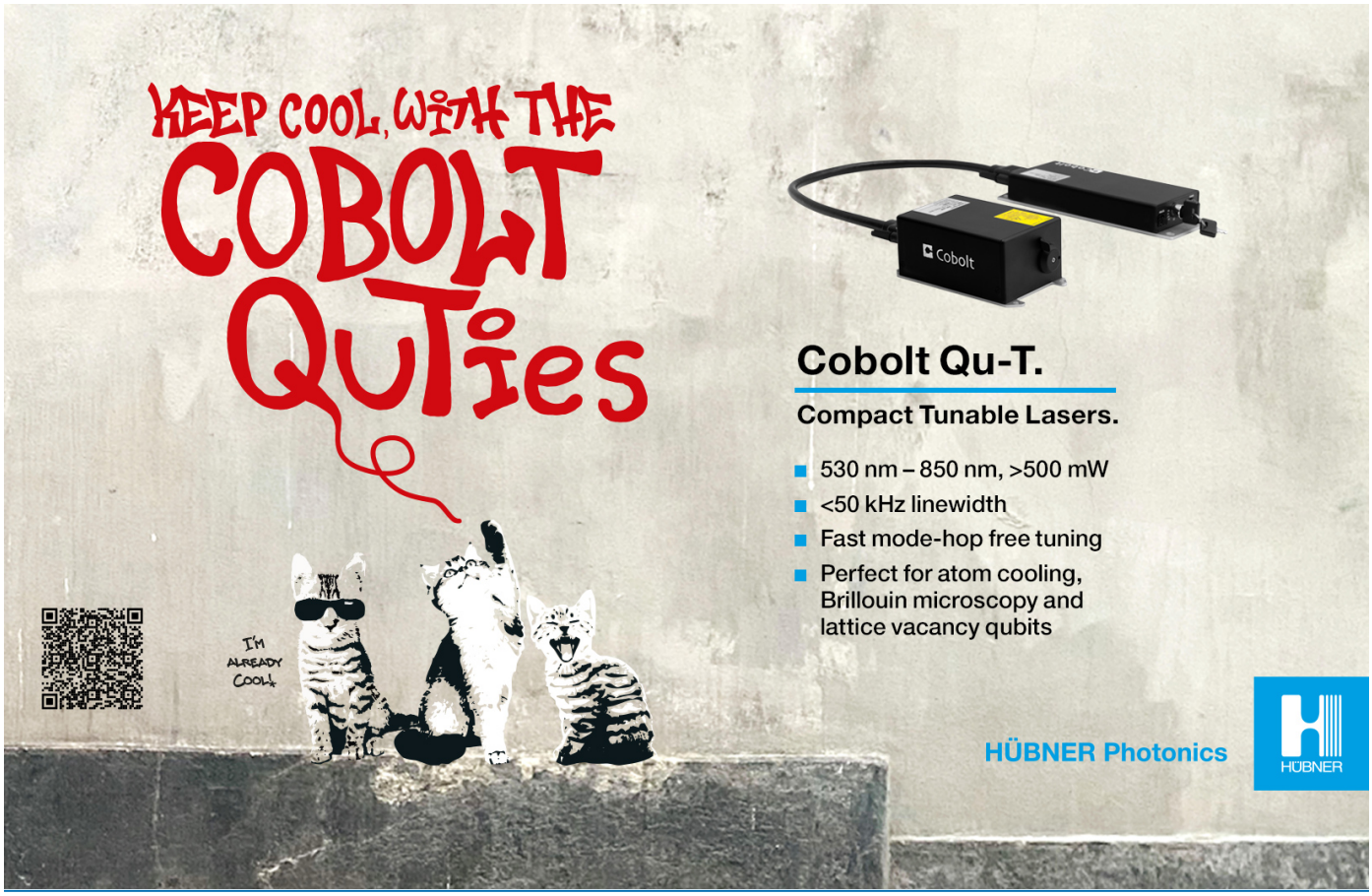

Quantum Science and Technology



OPEN ACCESS

RECEIVED
1 October 2025

REVISED
27 April 2026

ACCEPTED FOR PUBLICATION
10 June 2026

PUBLISHED
30 June 2026



PAPER

# Quantum lattice Boltzmann algorithm for heat transfer with phase change

**Christopher L Jawetz**[1], **Zhixin Song**[2], **Spencer H Bryngelson**[1,3] and **Alexander Alexeev**[1,*]

[1] George W. Woodruff School of Mechanical Engineering, Georgia Institute of Technology, Atlanta, GA 30332, United States of America
[2] School of Physics, Georgia Institute of Technology, Atlanta, GA 30332, United States of America
[3] School of Computational Science & Engineering, Georgia Institute of Technology, Atlanta, GA 30332, United States of America
[*] Author to whom any correspondence should be addressed.

**E-mail:** alexander.alexeev@me.gatech.edu

**Keywords:** quantum lattice Boltzmann, heat transfer, phase change

## Abstract

Heat transfer involving phase change is computationally intensive due to moving phase boundaries, nonlinear computations, and time step restrictions. This paper presents a quantum lattice Boltzmann method (QLBM) for simulating heat transfer with phase change. The approach leverages the statistical nature of the lattice Boltzmann method (LBM) while addressing the challenges of discontinuous phase transitions in quantum computing. The method implements an interface-tracking strategy that partitions the problem into separate solid and liquid domains, enabling the algorithm to handle the discontinuity in the enthalpy–temperature relationship. We store phase change information in the quantum circuit to reduce information exchange between classical and quantum hardware, a bottleneck in many quantum applications. Results from the implementation agree with both classical LBM and analytical solutions, demonstrating QLBM as an effective approach for analyzing thermal systems with phase transitions. Simulations using 17 lattice nodes with 53 qubits demonstrate temperature root-mean-square errors of order 0.01 when compared against classical solutions. The method accurately tracks interface movement during phase transition.

## 1. Introduction

Modeling phase transitions in materials presents computational challenges, particularly when tracking the evolving interfaces between solid and liquid states. The computational demands make such simulations promising candidates for quantum computing approaches, which could offer substantial speedups over classical methods. Classical computational approaches to phase change problems employ interface-handling strategies with different trade-offs. Fixed-enthalpy methods [1] reformulate the energy equation using enthalpy rather than temperature, avoiding explicit interface tracking but often introducing numerical diffusion. Direct interface-tracking approaches, including front-tracking methods [2] and fixed-grid transformations [3], maintain interface sharpness but require complex algorithms for topological changes. Alternative formulations such as level-set methods [4] and phase-field methods [5] offer different balances between accuracy and computational efficiency. Despite these advances, classical methods face scaling limitations. This paper develops a quantum lattice Boltzmann method (QLBM) for simulating heat transfer with phase change, focusing on implementing nonlinear phase transitions in a quantum computing context.

The lattice Boltzmann method (LBM), a mesoscale modeling approach based on solutions to the Boltzmann equation, offers advantages for quantum implementation [6]. LBM's inherent locality and statistical nature make it well-suited for quantum computing architectures. Multiphase LBM methods have evolved through several approaches to interface modeling. Gunstensen *et al* [7] developed a multicomponent flow method with surface tension derived from a secondary collision step. Shan and Chen [8] used a pseudopotential term to model surface tension between phases with an equation of state in

the equilibrium distribution. Free energy methods by Swift *et al* [9] later provided more consistent thermodynamic formulations. For phase change specifically, the implicit enthalpy method incorporates a phase change term in the collision operator to capture melting effects [10]. This approach avoids costly iterations but still faces computational limits on classical hardware.

In this context, quantum computing has emerged as an alternative to classical approaches for simulating complex physical systems. Recent advances in quantum hardware from IBM, Microsoft, and Google have improved qubit coherence times and gate fidelity, enabling more complex quantum algorithms [11–15]. Some algorithms offer potential exponential speedup over classical methods [16, 17]. The Harrow–Hassidim–Lloyd algorithm for solving linear systems exemplifies this potential [18]. More advanced quantum linear system algorithms [19] have been adopted to solve various linear PDEs. Combined with linearization techniques [20], these algorithms can also solve some nonlinear PDEs [6, 21, 22]. However, practical implementation on near-term quantum hardware faces limitations from quantum circuit depth. These solvers also require high-fidelity operations enabled by quantum error correction [23]. These challenges increase when extending the algorithm to nonlinear systems using linearization techniques, which expands the system size and circuit complexity.

Variational quantum algorithms represent another research direction for implementing quantum linear system solvers on near-term hardware [24, 25]. These algorithms use shallow, parameterized circuits and classical optimization to approximately solve linear systems. Their shallow depth and robustness against coherent noise make them suitable for noisy intermediate-scale quantum devices. Liu *et al* [26] solved the Laplace equation in one and two dimensions using this method, while Song *et al* [27] solved the incompressible Navier–Stokes equation and tested it on IBM's quantum computer.

Another approach has been through mesoscale modeling techniques such as the LBM, which are common in classical computing because of their speed and parallelizability. Yepez [28] developed the first quantum formulation. This quantum lattice-gas model mapped each velocity channel to a qubit and implemented streaming through SWAP gates and local BGK-like collisions through unitary transformations. Budinski [29] extended this work with the first complete circuit implementation. They used a linear combination of unitaries approach to implement the non-unitary collision operator and solve the advection–diffusion equation. Later, they applied the scheme to the stream-function–vorticity formulation of the Navier–Stokes equations [30]. To address collision nonlinearity, Itani and Succi [31] introduced Carleman linearization that embeds the BGK operator into a larger linear space. They recently produced a quantum algorithm for lattice Boltzmann implementing both streaming and collision steps as unitary operators [32]. Sanavio *et al* [33] explored the relative benefits of Carleman linearization using gate-based and block-encoding techniques.

Recent efforts for QLBM have focused on resource optimization and scalability. Kocherla *et al* [34] developed an algorithm that avoids repeated measurements and reinitialization between time steps. Lee *et al* [35] created a two-circuit streamfunction–vorticity algorithm that calculates quantum circuits concurrently and reduces CNOT gate count by 35% while maintaining $\mathcal{O}(\log N)$ scaling in qubit count. Wang *et al* [36] introduced a meso-ensemble method with smaller dimensionality than the full cellular automata model while achieving linear collisions. Other resource-reduction strategies include Kumar and Frankel [37]'s method to solve a timestep with a single unitary transformation and Wawrzyniak *et al* [38]'s sparse-matrix encoding, scaled to a $128 \times 128$ lattice on a statevector simulator. These prior QLBM studies address single-phase flows or multiphase coexistence, but none have tackled phase transitions involving latent heat absorption and moving boundaries. A key challenge in such problems is the frequent quantum–classical communication typically required by QLBM algorithms, which undermines potential quantum advantage.

The presented work focuses on whether quantum LBMs (QLBMs) can simulate heat transfer problems with phase change while minimizing measurement and reinitialization overhead. The approach introduces a quantum interface-tracking scheme inspired by classical enthalpy approaches to encode the liquid fraction and phase-boundary position as qubit registers. This scheme allows one to handle the discontinuous enthalpy–temperature mapping at melting. To our knowledge, this is the first approach to studying phase change problems through QLBM.

This manuscript continues as follows. Section 2 defines the Stefan problem. Section 3 describes the LBM and its adaptation for phase change. Section 4 describes the QLBM. Section 5 presents model additions to incorporate phase change. Section 6 presents the results, verifying the model against analytical and classical LBM solutions. Section 7 provides concluding remarks on the results and their significance.

## 2. Problem description

The analysis considers transient one-dimensional heat transfer with phase change in a finite solid wire at initial temperature $T_{\text{solid}}$, known as the Stefan problem [39]. At time $t = 0$, a constant temperature $T_{\text{bound}}$ is imposed at $x = 0$ as illustrated in figure 1. The bar melts at temperature $T_{\text{melt}}$ where $T_{\text{solid}} < T_{\text{melt}} < T_{\text{bound}}$ and creates a moving phase interface at position $x_{\text{I}}(t)$. The problem uses an enthalpy $H$ formulation

$$\frac{1}{c_p}\frac{\partial H}{\partial t} = \alpha \nabla^2 T, \tag{1}$$

where $\nabla^2$ is the spatial Laplacian, $\alpha$ is the thermal diffusivity, and $c_p$ is the specific heat capacity at constant pressure [1]. The enthalpy $H$ relates to temperature $T$ as

$$H = \begin{cases} c_p T, & T < T_{\text{melt}}, \\ c_p T + \mathcal{L}_{\text{melt}}, & T > T_{\text{melt}}, \end{cases} \tag{2}$$

where $\mathcal{L}_{\text{melt}}$ is the latent heat of melting. At $T = T_{\text{melt}}$, the function becomes discontinuous as enthalpy decouples from temperature. This decoupling creates a discontinuity in the relation between $H$ and $T$. This discontinuity complicates quantum algorithms as $T$ cannot be directly computed from $H$ without quantum measurements and classical computation, which collapses the quantum state.

Rubinstein [40] provides an analytical solution for the classical Stefan problem that tracks the moving phase boundary without a temperature–enthalpy inversion. The interface position is found as

$$x_{\text{I}}(t) = 2\lambda\sqrt{\alpha t}, \tag{3}$$

and the interface movement speed $\lambda$ follows from

$$\lambda\sqrt{\pi} = \frac{\text{St}_{\text{liq}}}{\exp(\lambda^2)\,\text{erf}(\lambda)} - \frac{\text{St}_{\text{solid}}}{\exp(\lambda^2)\,\text{erfc}(\lambda)}, \tag{4}$$

with erf$(\cdot)$ and erfc$(\cdot)$ the error and complementary error functions. The Stefan numbers St for liquid and solid phases are

$$\text{St}_{\text{liq}} = \frac{c_p(T_{\text{bound}} - T_{\text{melt}})}{\mathcal{L}_{\text{melt}}} \quad \text{and} \quad \text{St}_{\text{solid}} = \frac{c_p(T_{\text{melt}} - T_{\text{solid}})}{\mathcal{L}_{\text{melt}}}. \tag{5}$$

The liquid temperature is

$$T(x,t) = T_{\text{bound}} - (T_{\text{bound}} - T_{\text{melt}})\frac{\text{erf}\left(x/2\sqrt{\alpha t}\right)}{\text{erf}(\lambda)} \tag{6}$$

and the solid temperature is

$$T(x,t) = T_{\text{melt}}\frac{\text{erfc}\left(x/2\sqrt{\alpha t}\right)}{\text{erfc}(\lambda)}. \tag{7}$$

## 3. Computational model

Equation (1) can be solved using the LBM, a mesoscale modeling technique for transport equations [41]. Although the governing equations presented above are general for three-dimensional problems, we focus on the one-dimensional case for this study. LBM models heat transport using fictitious particles moving along a spatially fixed lattice. The particles are characterized by a probability density function $f_i(\mathbf{x}, t)$. The algorithm consists of collision and streaming steps. The collision procedure represents an instant collision of particles arriving from different lattice directions to a lattice node where they collide and relax toward a local equilibrium $f_i^{\text{eq}}$. The streaming procedure represents particles moving along lattice links in their respective directions.

The discrete Boltzmann equation describes the evolution of the distribution function $f_i$ as

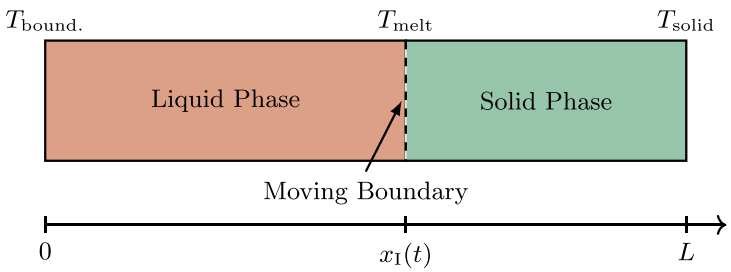


**Figure 1.** Schematic of a 1D phase change problem with a moving interface boundary. The domain of length $L$ contains liquid (left) and solid (right) phases separated by a moving boundary at $x_{\text{I}}(t)$. This setup illustrates the Stefan problem for melting processes.

$$f_i(\mathbf{x}+\mathbf{e}_i\Delta t, t+\Delta t) = (1-\omega\Delta t) f_i(\mathbf{x},t) + \omega\Delta t f_i^{\text{eq}} - w_i\Phi, \tag{8}$$

where $\mathbf{x}$ is the lattice position vector, $\Delta t$ is the time step, $f_i^{\text{eq}}$ is the equilibrium distribution function, $\omega$ is the relaxation coefficient, and $\mathbf{e}_i$ is the lattice velocity vector for direction $i$. The source term is related to the latent heat of melting as

$$\Phi = \frac{\mathrm{d}\eta}{\mathrm{d}t}\frac{\mathcal{L}_{\text{melt}}}{c_p}\delta(T-T_{\text{melt}}). \tag{9}$$

Here, $\eta$ is the liquid fraction at the lattice node, and $\delta(\cdot)$ is the Dirac delta function that accounts for latent heat absorption during phase change [1]. The implementation uses a time step of $\Delta t = 1$ and lattice spacing of $\Delta x = 1$, and all quantities are nondimensionalized using the reference state variables. The model uses a one-dimensional, three-velocity (D1Q3) lattice, where the velocity vectors are $\mathbf{e}_0 = 0$, $\mathbf{e}_1 = -1$, and $\mathbf{e}_2 = +1$, incorporating rest particles and motion in both directions, creating a balanced lattice structure for stability and isotropy. The relaxation coefficient $\omega = 2/(6\alpha + \Delta t)$ is a measure of thermal diffusivity [10].

The macroscopic temperature $T$ is calculated from the distribution function as

$$T(\mathbf{x},t) = \sum_{i=0}^{2} f_i(\mathbf{x},t). \tag{10}$$

The equilibrium distribution function is $f_i^{\text{eq}}(\mathbf{x},t) = w_i T(\mathbf{x},t)$, with weights $\mathbf{w} = [1/6,\ 2/3,\ 1/6]^\top$. The source term $\Phi$ is zero everywhere except at $T = T_{\text{melt}}$. At $T = T_{\text{melt}}$, we calculate $\Phi$ by computing $f_i(\mathbf{x}, t+\Delta t)$ without $\Phi$, then setting

$$\Phi = \sum_{i=0}^{2} f_i(\mathbf{x}, t+\Delta t) - T_{\text{melt}}. \tag{11}$$

This relationship enables the liquid fraction change to be evaluated using equation (9). We scale $f_i(\mathbf{x}, t+\Delta t)$ so that $\sum_{i=0}^{2} f_i(\mathbf{x}, t+\Delta t) = T_{\text{melt}}$, preserving energy balance at the interface. We store the liquid fraction with the temperature, so the enthalpy $H$ is

$$H = c_p T + \mathcal{L}_{\text{melt}}\eta, \tag{12}$$

corresponding to the enthalpy relation in equation (2). We track interface position $x_{\text{I}}$ with sub-grid precision as

$$x_{\text{I}} = x + (\eta - 0.5)\Delta x, \tag{13}$$

within the melting node at position $x$.

The one-dimensional domain is $x \in [0, L]$ with constant temperature boundary conditions $T(x = 0, t) = T_{\text{bound}}$ and $T(x = L, t) = T_{\text{solid}}$. For lattice directions entering from outside the domain, we compute the unknown distribution function values by preserving the boundary temperature as

$$f_j = T - \sum_{i\neq j} f_i, \tag{14}$$

where $f_j$ is the distribution function for lattice direction $j$.

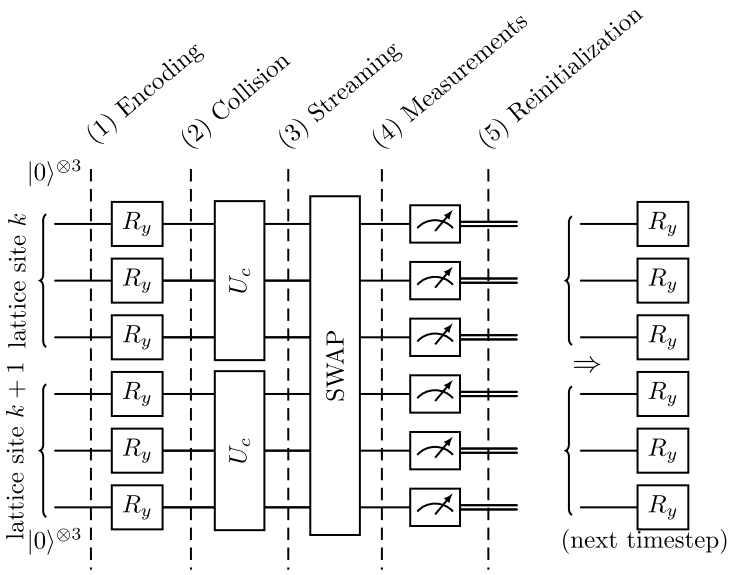


**Figure 2.** Quantum circuit for a single time step of the QLBM algorithm between lattice sites $k$ and $k+1$ under the D1Q3 scheme. The overall circuit operates on $3N$ qubits initially in the $|0\rangle$ state, where $N$ is the total number of lattice sites. Each time step includes five stages: (1) encoding: initialization of qubit states to represent particle distribution functions using $R_y$ gates, (2) collision: unitary collision operators $U_c$ modeling particle interactions inside each lattice node $k$, (3) streaming: particle propagation using SWAP operations between adjacent lattice sites, (4) measurement: measure the quantum states to retrieve $f_i$; and (5) reinitialization: prepare the initial quantum state for the next time step based on distribution from previous time step and enforcing boundary conditions.

## 4. Quantum algorithm

Yepez [28] introduced the first QLBM. A measurement-based algorithm encodes each particle at each lattice node as a qubit. The approach is shown in figure 2, where each quantum gate represents a specific operation in the QLBM algorithm. The circuit involves $R_y$ gates, which perform $Y$-rotations for encoding particle distribution functions into quantum states using angle $\theta_{k,i} = 2\cos^{-1}(\sqrt{1-f_i(x_k,t)})$. The unitary collision operator $U_c$ models particle interactions during the collision step. SWAP gates implement the streaming operation for particle propagation between neighboring lattice sites.

The algorithm begins with encoding. We encode initial temperature distribution values into registers, with the interface node encoded in a separate register. Each qubit encodes the distribution value $f_i$ as

$$|q_i(x_k,t)\rangle = \sqrt{1-f_i(x_k,t)}\,|0\rangle + \sqrt{f_i(x_k,t)}\,|1\rangle, \quad k=0,1,2,\ldots,N-1, \quad i=0,1,2, \tag{15}$$

where $N$ is the total number of lattice sites, $k$ is the lattice site index, and $i$ is the velocity direction index. We implement this using an $R_y(\theta_{k,i})$ gate with angle $\theta_{k,i} = 2\cos^{-1}(\sqrt{1-f_i(x_k,t)})$ for the ket vector $|q_i(x_k,t)\rangle$. The state at lattice site $k$ is

$$|\psi(x_k,t)\rangle = |q_0(x_k,t)\rangle \otimes |q_1(x_k,t)\rangle \otimes |q_2(x_k,t)\rangle. \tag{16}$$

Hence, the overall quantum state is a product state of each lattice site state as

$$|\psi(x_0,x_1,\cdots,x_{N-1},t)\rangle = \bigotimes_{k=0}^{N-1} |\psi(x_k,t)\rangle. \tag{17}$$

The QLBM collision operation $U_c$ applies a unitary transformation to each lattice node $|\psi(x_k,t)\rangle$, relaxing the distribution toward equilibrium analogous to the BGK operator in classical LBM. The operator for D1Q3 is an expansion of the collision operator described in Yepez [42] for the D1Q2 scheme. To conserve energy within the node during the collision, this operator disjointly entangles the states with equal Hamming weights: $\mathcal{S}_1 = \{|001\rangle, |010\rangle, |100\rangle\}$ and $\mathcal{S}_2 = \{|011\rangle, |101\rangle, |110\rangle\}$, each having respectively one or two qubits in $|1\rangle$. Mixing only within these subspaces redistributes the distribution functions while preserving their sum: the quantum analog of conserving energy in the classical LBM collision step. Thus, the $8\times 8$ matrix $U_c$ is described via two SU(3) unitary group block matrices, which represent

the disjoint mixing processes, along with unitary values for $|000\rangle$ and $|111\rangle$. Particle-hole symmetry is enforced with a global NOT operation on the second set of states $\mathcal{S}_2$ using a permutation matrix

$$P = \begin{bmatrix} 0 & 0 & 1 \\ 0 & 1 & 0 \\ 1 & 0 & 0 \end{bmatrix}. \tag{18}$$

Then, we can write the collision operator $U_c$ as the direct sum of each component

$$U_c = 1 \oplus V \oplus PVP^{\dagger} \oplus 1. \tag{19}$$

Imposing isotropy on the link directions limits $V$ to linear combinations of the identity matrix $I_{3\times3}$ and the all-ones matrix $J_{3\times3}$ (normalized to satisfy unit trace $\mathrm{Tr}[J] = 1$) as

$$V = \alpha J + \beta (I - J). \tag{20}$$

We require $|\alpha| = |\beta| = 1$ to preserve unitarity, resulting in a free parameter $\alpha = 1, \beta = \exp(i\theta)$. We choose $\theta = 2\pi/3$ to maximize the mixing between the three quantum states in each subspace, corresponding to $\omega = 6/5$ in standard LBM heat transfer models. After reframing the result in the canonical basis, we obtain

$$U_c = \frac{1}{\sqrt{3}} \begin{bmatrix} \sqrt{3} & 0 & 0 & 0 & 0 & 0 & 0 & 0 \\ 0 & \mathrm{i} & \exp(-\mathrm{i}\pi/6) & \exp(-\mathrm{i}\pi/6) & 0 & 0 & 0 & 0 \\ 0 & \exp(-\mathrm{i}\pi/6) & \mathrm{i} & \exp(-\mathrm{i}\pi/6) & 0 & 0 & 0 & 0 \\ 0 & 0 & 0 & 0 & \exp(-\mathrm{i}\pi/6) & \exp(-\mathrm{i}\pi/6) & \mathrm{i} & 0 \\ 0 & \exp(-\mathrm{i}\pi/6) & \exp(-\mathrm{i}\pi/6) & i & 0 & 0 & 0 & 0 \\ 0 & 0 & 0 & 0 & \exp(-\mathrm{i}\pi/6) & i & \exp(-\mathrm{i}\pi/6) & 0 \\ 0 & 0 & 0 & 0 & \mathrm{i} & \exp(-\mathrm{i}\pi/6) & \exp(-\mathrm{i}\pi/6) & 0 \\ 0 & 0 & 0 & 0 & 0 & 0 & 0 & \sqrt{3} \end{bmatrix}. \tag{21}$$

The streaming operation uses the established quantum walk algorithm, permuting qubits via SWAP gates [29]. Last, we reset the qubit phases to restore the post-initialization state. The results of section 6 show that one can advance multiple time steps without reinitialization. By reducing reinitialization, one also reduces repeated state preparation and readout of solution states, which can introduce noise that accumulates with each measurement–reinitialization cycle.

## 5. QLBM with phase change

To incorporate phase change, we separate the system into two registers at the melting node, each containing a copy of the temperature field as shown in figure 3. The system wavefunction for the liquid region is

$$\left|\Psi\left(x_0, x_1, \ldots, x_{N_{\mathrm{liq}}-1}, t\right)\right\rangle = \bigotimes_{k=0}^{N_{\mathrm{liq}}-1} |\psi(x_k, t)\rangle \tag{22}$$

and for the solid region is

$$\left|\Psi\left(x_{N_{\mathrm{liq}}-1}, x_{N_{\mathrm{liq}}}, \ldots, x_{N-1}, t\right)\right\rangle = \bigotimes_{k=N_{\mathrm{liq}}-1}^{N-1} |\psi(x_k, t)\rangle \tag{23}$$

for a period with $N_{\mathrm{liq}}$ liquid sites and $N - N_{\mathrm{liq}}$ solid sites. This partitioning strategy addresses the discontinuity in the enthalpy-temperature relationship. Within each register, the relationship $H = c_p T$ remains continuous and single-valued. The discontinuous jump of $\mathcal{L}_{\mathrm{melt}}$ at the melting point is isolated to the

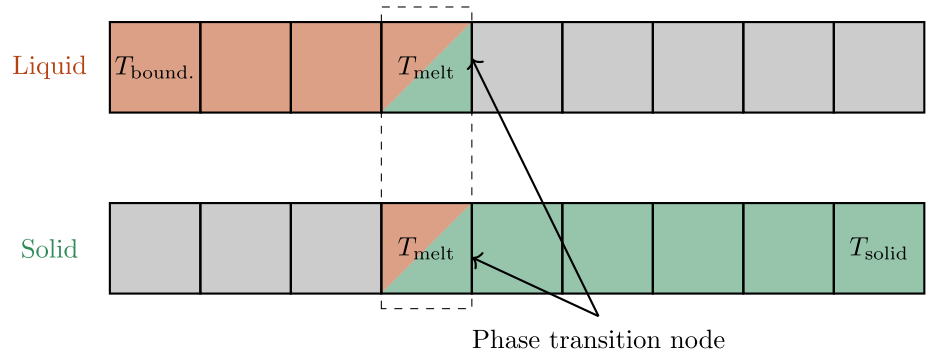


**Figure 3.** The discretization scheme for the phase change problem shows grids for two phases (brown, liquid; green, solid). The phase boundary is indicated in the dashed box. The boundary conditions are $T_{\text{bound}}$ and $T_{\text{solid}}$ for the left and right boundaries. The grayed-out nodes are for illustrative purposes, as each phase only exists in one of the two grids or the phase change node, and so are not used in the calculations.

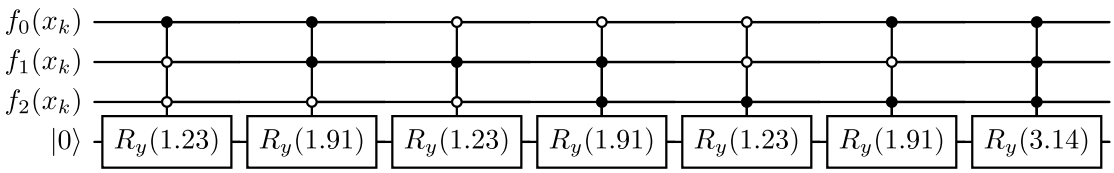


**Figure 4.** MCRY circuit evaluates possible measurement combinations at each lattice node, shown for the distributions $f_i$, by rotating the ancilla qubit. Rotation angles are determined by the sum $S$ of control values.

interface node, where we track the liquid fraction $\eta$ classically rather than requiring the quantum circuit to invert the relationship between $H$ and $T$ across the discontinuity. This approach allows the quantum algorithm to solve continuous heat diffusion in each phase while the phase-change nonlinearity is handled by classically tracking the accumulated latent heat.

We implement a multi-controlled rotation (MCRY) gate sequence at the liquid–solid interface to measure post-streaming temperature within the circuit. This circuit, shown in figure 4, systematically evaluates all possible measurement combinations at each node, applying specific rotation angles to encode temperature information in an ancilla qubit's probability amplitude. The rotation angle $\theta = 2\sin^{-1}(\sqrt{S/3})$ ensures the ancilla qubit yields 1 with probability $S/3$, where $S$ represents the sum of control bit values. This procedure produces a single rotation each timestep with an amplitude corresponding to the measured value. The mapping creates a linear correspondence between measured probability and temperature $T$.

The circuit rotation angles correspond to possible combinations of the three input qubits representing discrete temperature distributions. The corresponding numerical values (1.23, 1.91, and so on) are computed from the inverse sine function applied to the square root of the normalized sum of control values, scaled to match the expected temperature range at the phase interface. We scale the probability amplitude by $\mathcal{L}_{\text{melt}}((S/3) - T_{\text{melt}})/c_p$ to compute the liquid fraction change, which is applied after measurement.

The MCRY circuit stores information without disrupting the superposition of other qubits, as shown in figure 5. This QLBM approach is an improvement over traditional QLBM methods, isolating the discontinuous phase change contribution without collapsing the quantum state. The ancilla qubits are only required at the interface nodes, resulting in 2 qubits for the 1D case and a total qubit count of $3N+2$ for $N$ lattice sites. This hybrid quantum–classical approach enables efficient phase-change simulation while preserving the quantum coherence of the primary computation. The measured phase change information propagates through later time steps via classical tracking of the liquid fraction: the interface position is evaluated using equation (13) and the liquid fraction from the enthalpy balance in equation (12).

The implementation requires a different approach to the boundary conditions. Each time step produces one unknown lattice direction at fixed boundaries, traditionally calculated using known boundary values. This calculation cannot rely on direct boundary-value observations without intermediate measurements.

In regions undergoing phase change, we heuristically assume that the melting node exhibits quasi-static behavior, enabling previous boundary condition values to be used. This assumption is supported

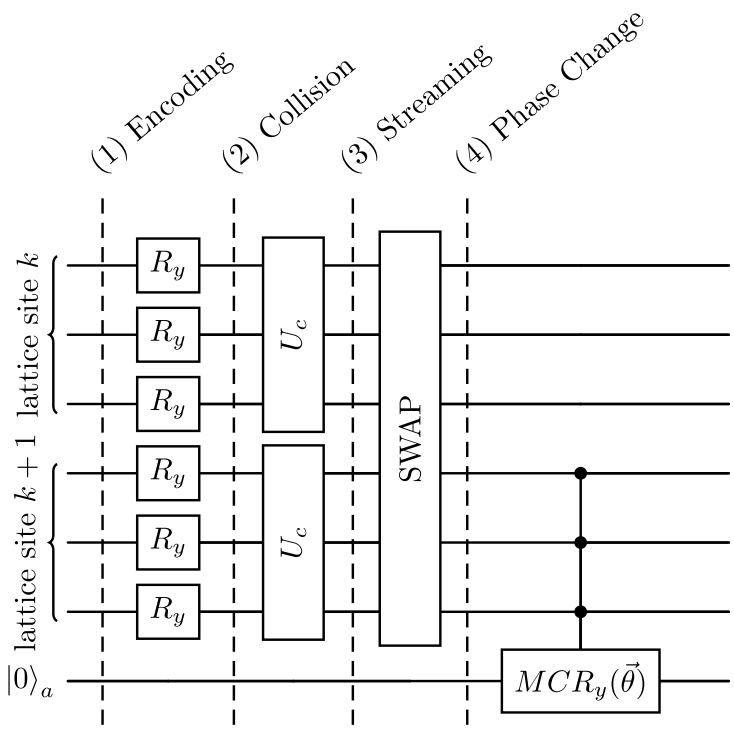


**Figure 5.** QLBM circuit, using the MCRY gate to store phase change data from the boundary lattice site. Circuit symbols: $R_y$ are $Y$-rotation gates; $U_c$ is the unitary collision operator; $C$ denotes control qubits; and $\mathrm{MCR}_y(\vec{\theta})$ is the multi-controlled rotation gate for phase change detection.

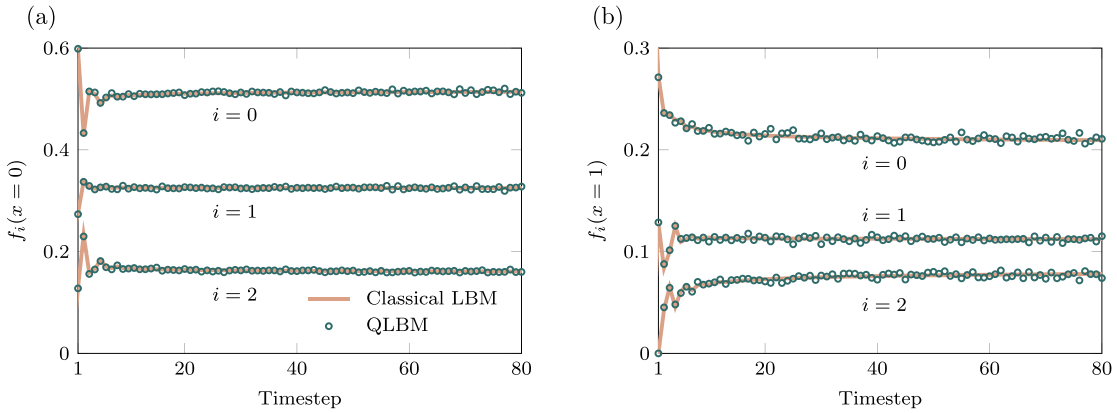


**Figure 6.** Time evolution of LBM distribution function values at (a) the left boundary and (b) the phase interface. Distributions $f_i$ along different lattice directions $i$ are shown as labeled. We limit this to the initial phase ($t \in [0, 80]$) to demonstrate the settling effect and quasi-static behavior.

empirically by comparing quantum and classical solutions in figure 6, which shows close agreement. In figures 6(a) and (b), the values of the distribution functions $f_i$ are shown at the left boundary and the node undergoing melting, respectively; the time steps here denote the time after phase change moves into the labeled node (grid cell). The distribution functions reach approximately steady values within about 5 time steps, after which we no longer need to recompute boundary condition values. This quasi-static region arises from the constant temperature at the interface, which reduces the effect of heat flux into and out of the node on the distribution values. On the liquid side, the prolonged melting at each node allows the surrounding temperature field to approach a quasi-steady profile, so the incoming distribution is nearly stationary. On the solid side, the incoming distribution propagates against the primary heat flux direction, and its magnitude is small relative to the other distributions, so its temporal variation is also small. Information transfer between the solid and liquid registers also occurs classically between reinitializations, through the standard LBM streaming procedure. As the liquid fraction approaches 1, the system reverts to the original algorithm until distribution function values reach an

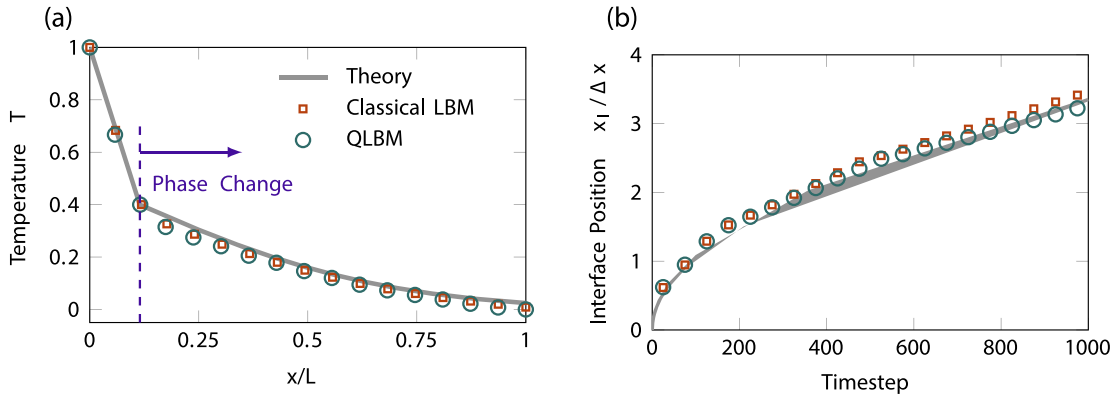


**Figure 7.** Comparison between the analytic solution, classical LBM, and quantum LBM (this work) methods. (a) Temperature distribution after 300 time steps, equivalent to $t = 300$. The vertical dashed line indicates the interface location as predicted by theory. (b) Interface position evolution. The interface position is determined by the current melting node along with the liquid fraction at that node.

approximate steady state. Still, the phase interface moves through the domain as the simulation progresses ($t \in [0, 80]$, here). Thus, this test provides a faithful physical benchmark for algorithm performance evaluation.

We use linear extrapolation of the liquid fraction to predict complete melting at a lattice node, which behaves linearly because of constant boundary conditions. When the melting node changes, the system reverts to per-time-step measurements until reaching an updated equilibrium state. The transition period duration varies with thermal diffusivity $\alpha$ but remains short for typical metal values.

## 6. Results

Figure 7 compares the analytic solution, classical LBM solution, and QLBM solution for one-dimensional heat transfer along a bar with $T_{\text{melt}} = 0.4\,T_{\text{bound}}$ and $\mathcal{L}_{\text{melt}}/c_p = 10$. We chose parameters to examine phase change behavior in a moderate temperature regime, with the melting point positioned away from boundaries. The simulation uses 17 lattice nodes with 53 qubits, which provides a practical balance between spatial resolution and the number of qubits. We perform QLBM simulations via the Qiskit Aer MPS simulator [43] for 1000 time steps ($t \in [0, 1000]$).

We find close agreement between the classical and quantum solutions in terms of temperature distribution shown in figure 7(a) and interface position evolution shown in figure 7(b), confirming that QLBM can properly solve this problem and represent the interface dynamics. The results show good agreement between all solutions for the temperature $T(x)$. Additionally, the classical LBM model converges to the theoretical solution with grid refinement, though this is not yet practical for the quantum algorithm.

The interface evolution in figure 7(b) shows that the simulations using the quantum algorithm represent the phase change dynamics with small errors. The quantum solution tracks the classical result throughout the phase transition period, representing the initiation and progression of the phase change. This agreement demonstrates an effective approach to representing discontinuous phase change behavior in a quantum computing context. Furthermore, the interface position predicted by the quantum solution closely follows the analytical solution $x_{\text{I}}(t)$ given in equation (3).

Error analysis of the quantum solutions is shown in figure 8, highlighting key characteristics of the implementation's performance. We evaluate the error between the quantum circuit and classical LBM solutions. The absolute root mean square (RMS) error for a quantity $q$ is defined as

$$E_{\text{RMS}} = \sqrt{\frac{1}{M}\sum_{k=1}^{M}\left(q^{(k)}_{\text{classical}} - q^{(k)}_{\text{quantum}}\right)^2}, \tag{24}$$

where $k$ is the lattice site index and $M = 17$ is the total number of lattice sites.

The error for temperature $T$ remains below 0.01 throughout the simulation except for transient spikes where the melting node transitions to the following mesh node. The interface location $x_{\text{I}}$ error slowly increases in time as the simulation progresses and saturates at larger $t$. This error is due entirely

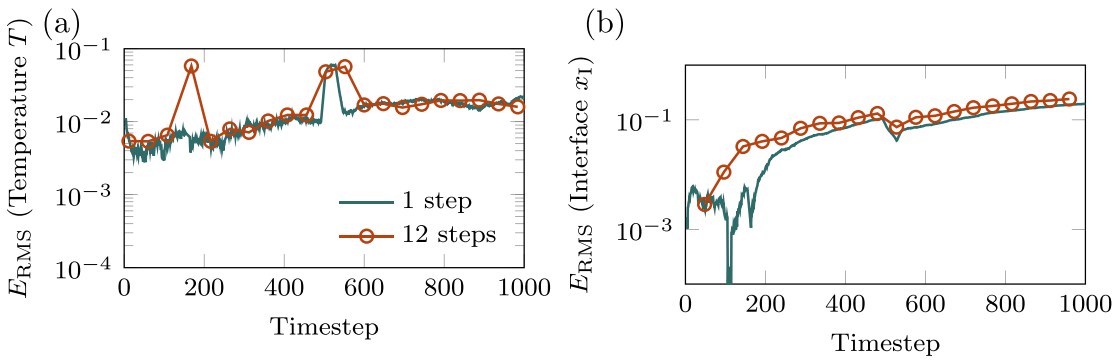


**Figure 8.** Error results comparing quantum and classical LBM solutions and reinitialization schemes. The RMS error follows equation (24) for (a) temperature $T$ and (b) interface position $x_1$. The temporary spikes around time steps 200 and 600 are due to transient effects as the melting node changes.

to the quantum implementation, as both the classical and quantum algorithms use the same grid eliminating the effect of discretization error. Examination of the maximum absolute error and the error distribution across the domain demonstrates that the majority of the error is concentrated near the interface early on, with a more even distribution as the simulation progresses. The relative and absolute RMS errors are similar in scale, so we do not show both here. Importantly, the 12-step model does not exhibit meaningfully higher error in either regard, demonstrating the effectiveness of the approach. This interval was determined empirically and can be further extended depending on the problem parameters. The optimal reinitialization frequency depends on parameters such as the Stefan number and thermal diffusivity, which govern interface velocity and the duration of quasi-static behavior at each node. Our result demonstrates that extended reinitialization intervals are feasible for this nonlinear problem.

## 7. Conclusions

This paper presents a QLBM for heat transfer with phase change. The method demonstrates how quantum algorithms can handle the discontinuity arising from phase change and reduce the computational burden of repeated reinitialization. Further, using a variable source term via an enthalpy-based formulation extends the method to represent phase change dynamics.

Results show that the presented QLBM technique accurately represents heat transfer with phase change, as verified by comparisons to classical LBM simulations and analytical solutions. Using the D1Q3 lattice, quantum simulations replicate temperature distribution and liquid fraction evolution during phase transition. Because the phase-change and boundary-condition information is captured within the circuit, the method can advance for several time steps without reinitialization. Reducing reinitialization count increases computational efficiency at a cost linear in the additional qubits. The differences between quantum, classical, and analytical solutions remain small across all tests.

Although the QLBM algorithm was originally designed for fault-tolerant quantum computers that can run millions of high-fidelity quantum operations [44], recent work shows that heavy optimization on the algorithm and circuit design can realize simple QLBM runs on current quantum hardware [45]. Adopting those recent developments and the idea of minimizing frequent measurements would further reduce the computational overhead of our QLBM algorithm, making the method more practical for early fault-tolerant quantum computers. Quantum computing's inherent parallelism opens possibilities for solving complex PDE-based problems more efficiently than classical methods alone. In this case, we show the technique is well-suited to heat transfer problems with phase transitions.

The method naturally extends to two- and three-dimensional problems by using higher-dimensional lattice structures (for example, D2Q9 or D3Q19), although the effects of fluid convection may need to be incorporated into the solution of higher-dimensional problems. Fluid convection could also be incorporated in a future model using the double distribution function approach standard in classical LBM, where a second set of distributions handles the momentum field. Existing QLBM solvers for fluid velocity can be coupled with the thermal algorithm following this same structure. Materials with temperature-dependent properties could be incorporated using more frequent updates to the collision operator, while multiple phase transitions generalize naturally through the inclusion of extra domain registers and interface nodes with proportional qubit overhead.

In higher dimensions, qubit requirements scale as $qN^d + 2N^{d-1}$ where $q$ is the number of velocities in the lattice model, $N$ is the number of lattice sites per side, and $d$ is the dimension of the problem. Gate count scales with $N^d q$ for encoding, collision, and streaming, and $N^{d-1}2^q$ for the phase transition and interface, meaning this method is particularly effective for large domains. Since collision and streaming are local operations, the circuit depth and the per-node collision operator, which is a fixed-size unitary ($8 \times 8$ for D1Q3), remains independent of system size. A 2D simulation on a $64 \times 64$ grid with D2Q9 would need roughly $64^2 \times 9 + 2 \times 64 = 36,992$ qubits. The scaling benefits of reinitialization depend on the specifics of the problem, and the question of the maximum potential benefit is an important topic for future investigations.

This work demonstrates QLBM's suitability for solving complex heat transfer problems with phase change, which are relevant to diverse engineering applications, including thermal management, energy storage, and additive manufacturing. Addressing the discontinuous enthalpy–temperature coupling and reducing computational overhead advances the application of quantum computing to simulating physical systems, extending beyond previously explored systems. These results suggest QLBM extends to a broader range of engineering applications, potentially offering speedups compared to classical methods.

## Acknowledgments

This work was supported by the CRNCH Fellowship from the Georgia Institute of Technology and the National Science Foundation via Grant No. CBET-2217647.

## Data availability statement

The code for this paper is available at: https://github.com/comp-physics/Quantum_Heat_LBM.

## Author contributions

Christopher L Jawetz 0009-0003-7110-1757
Conceptualization (equal), Data curation (lead), Formal analysis (lead), Investigation (equal), Methodology (lead), Software (lead), Validation (lead), Writing – original draft (lead), Writing – review & editing (equal)

Zhixin Song
Conceptualization (equal), Data curation (supporting), Investigation (equal), Formal analysis (supporting), Methodology (supporting), Software (supporting), Writing – original draft (supporting), Writing – review & editing (equal)

Spencer H Bryngelson 0000-0003-1750-7265
Conceptualization (equal), Funding acquisition (equal), Investigation (equal), Methodology (supporting), Project administration (equal), Supervision (equal), Writing – original draft (supporting), Writing – review & editing (equal)

Alexander Alexeev 0000-0002-8285-0003
Conceptualization (equal), Data curation (supporting), Funding acquisition (equal), Methodology (supporting), Investigation (equal), Project administration (equal), Supervision (equal), Writing – original draft (supporting), Writing – review & editing (equal)

## References

[1] Voller V R and Cross M 1981 Accurate solutions of moving boundary problems using the enthalpy method *Int. J. Heat Mass Transfer* **24** 545–56
[2] Unverdi S O and Tryggvason G 1992 A front-tracking method for viscous, incompressible, multi-fluid flows *J. Comput. Phys.* **100** 25–37
[3] Voller V R, Swaminathan C R and Thomas B G 1990 Fixed grid techniques for phase change problems: a review *Int. J. Numer. Methods Eng.* **30** 875–98
[4] Chen S, Merriman B, Osher S and Smereka P 1997 A simple level set method for solving Stefan problems *J. Comput. Phys.* **135** 8–29
[5] Karma A and Rappel W-J 1996 Phase-field method for computationally efficient modeling of solidification with arbitrary interface kinetics *Phys. Rev. E* **53** R3017

[6] Li X, Yin X, Wiebe N, Chun J, Schenter G K, Cheung M S and Mülmenstädt J 2025 Potential quantum advantage for simulation of fluid dynamics *Phys. Rev. Res.* **7** 013036
[7] Gunstensen A K, Rothman D H, Zaleski S and Zanetti G 1991 Lattice Boltzmann model of immiscible fluids *Phys. Rev. A* **43** 4320
[8] Shan X and Chen H 1993 Lattice Boltzmann model for simulating flows with multiple phases and components *Phys. Rev. E* **47** 1815
[9] Swift M R, Osborn W R and Yeomans J M 1995 Lattice Boltzmann simulation of nonideal fluids *Phys. Rev. Lett.* **75** 830
[10] Eshraghi M and Felicelli S D 2012 An implicit lattice Boltzmann model for heat conduction with phase change *Int. J. Heat Mass Transfer* **55** 2420–8
[11] Gupta R S *et al* 2024 Encoding a magic state with beyond break-even fidelity *Nature* **625** 259–63
[12] Microsoft Azure Quantum *et al* 2025 Interferometric single-shot parity measurement in InAs–Al hybrid devices *Nature* **638** 651–5
[13] Google 2025 Quantum AI and collaborators. Quantum error correction below the surface code threshold *Nature* **638** 920–6
[14] Kikuchi Y, Keever C M, Coopmans L, Lubasch M and Benedetti M 2023 Realization of quantum signal processing on a noisy quantum computer *npj Quantum Inf.* **9** 93
[15] Robledo-Moreno J *et al* 2025 Chemistry beyond the scale of exact diagonalization on a quantum-centric supercomputer *Sci. Adv.* **11** eadu9991
[16] Shor P W 1994 Algorithms for quantum computation: discrete logarithms and factoring *Proc. 35th Annual Symp. on Foundations of Computer Science* (IEEE) pp 124–34
[17] Gidney C 2025 How to factor 2048 bit RSA integers with less than a million noisy qubits (arXiv:2505.15917)
[18] Harrow A W, Hassidim A and Lloyd S 2009 Quantum algorithm for linear systems of equations *Phys. Rev. Lett.* **103** 150502
[19] Morales M E S, Pira L, Schleich P, Koor K, Costa P, An D, Aspuru-Guzik A, Lin L, Rebentrost P, and Berry D W 2024 Quantum linear system solvers: a survey of algorithms and applications (arXiv:2411.02522)
[20] Kowalski K and Steeb W 1991 *Nonlinear Dynamical Systems And Carleman Linearization* (World Scientific Publishing Company)
[21] Liu J-P, Kolden H O, Krovi H K, Loureiro N F, Trivisa K and Childs A M 2021 Efficient quantum algorithm for dissipative nonlinear differential equations *Proc. Natl Acad. Sci.* **118** e2026805118
[22] Liu J-P, An D, Fang D, Wang J, Low G H and Jordan S 2023 Efficient quantum algorithm for nonlinear reaction–diffusion equations and energy estimation *Commun. Math. Phys.* **404** 963–1020
[23] Zheng M, Liu C, Stein S, Li X, Mülmenstädt J, Chen Y and Li A 2024 An early investigation of the HHL quantum linear solver for scientific applications (arXiv:2404.19067)
[24] Cerezo M *et al* 2021 Variational quantum algorithms *Nat. Rev. Phys.* **3** 625–44
[25] Bravo P C 2022 Variational quantum architectures: applications for noisy intermediate-scale quantum computers *PhD Thesis* (Universitat de Barcelona)
[26] Liu Y, Chen Z, Shu C, Chew S C, Khoo B C, Zhao X and Cui Y D 2022 Application of a variational hybrid quantum–classical algorithm to heat conduction equation and analysis of time complexity *Phys. Fluids* **34** 117–21
[27] Song Z, Deaton R, Gard B and Bryngelson S H 2025 Incompressible Navier–Stokes solve on noisy quantum hardware via a hybrid quantum–classical scheme *Comput. Fluids* **288** 106507
[28] Yepez J 2001 Quantum lattice-gas model for computational fluid dynamics *Phys. Rev. E* **63** 046702
[29] Budinski L 2021 Quantum algorithm for the advection-diffusion equation simulated with the lattice Boltzmann method *Quantum Inf. Process.* **20** 57
[30] Budinski L 2022 Quantum algorithm for the Navier–Stokes equations by using the streamfunction-vorticity formulation and the lattice Boltzmann method *Int. J. Quantum Inf.* **20** 2150039
[31] Itani W and Succi S 2022 Analysis of Carleman linearization of lattice Boltzmann *Fluids* **7** 24
[32] Itani W, Sreenivasan K R and Succi S 2024 Quantum algorithm for lattice Boltzmann (QALB) simulation of incompressible fluids with a nonlinear collision term *Phys. Fluids* **36** 017112
[33] Sanavio C, Simon W A, Ralli A, Love P and Succi S 2025 Carleman-lattice-Boltzmann quantum circuit with matrix access oracles *Phys. Fluids* **37** 037123
[34] Kocherla S, Song Z, Chrit F E, Gard B, Dumitrescu E F, Alexeev A and Bryngelson S 2024 Fully quantum algorithm for mesoscale fluid simulations with application to partial differential equations *AVS Quantum Sci.* **6** 033806
[35] Lee M, Song Z, Kocherla S, Adams A, Alexeev A and Bryngelson S H 2025 A multiple-circuit approach to quantum resource reduction with application to the quantum lattice Boltzmann method *Future Gener. Comput. Syst.* **174** 107975
[36] Wang B, Meng Z, Zhao Y and Yang Y 2025 Quantum lattice Boltzmann method for simulating nonlinear fluid dynamics *npj Quantum Inf.* **11** 196
[37] Kumar E D and Frankel S H 2025 Quantum unitary matrix representation of the lattice Boltzmann model for low Reynolds fluid flow simulation *AVS Quantum Sci.* **7** 013802
[38] Wawrzyniak D, Winter J, Schmidt S, Indinger T, Schramm U, Janßen C, and Adams N A 2024 Unitary quantum algorithm for the lattice-Boltzmann method (arXiv:2405.13391)
[39] Alexiades V and Solomon A D 1993 *Mathematical Modeling of Melting and Freezing Processes* (Taylor & Francis)
[40] Rubinstein L I 1971 *The Stefan Problem* (American Mathematical Society, United States)
[41] Chen S and Doolen G 1998 Lattice Boltzmann method for fluid flows *Annu. Rev. Fluid Mech.* **30** 329–64
[42] Yepez J 2002 Quantum lattice-gas model for the Burgers equation *J. Stat. Phys.* **107** 203–24
[43] Javadi-Abhari A et al Quantum computing with Qiskit 2024 (arXiv:2405.08810)
[44] Preskill J 2025 Beyond NISQ: the Megaquop machine *ACM Trans. Quantum Comput.* **6** 1–7
[45] Tiwari A, Iaconis J, Jojo J, Ray S, Roetteler M, Hill C and Pathak J 2025 Algorithmic advances towards a realizable quantum lattice Boltzmann method *2025 IEEE Int. Conf. on Quantum Computing and Engineering (QCE)* vol 1 (IEEE) pp 2441–51